23. A. Mabuchi, K. Tokumitsu, H. Fujimoto, and T. Kasuh, *ibid.*, **142,** 1041 (1995).
24. T. Zheng, J. N. Reimers, and J. R. Dahn, *Phys. Rev.*, **B51,** 734 (1995).
25. T. Zheng and J. R. Dahn, *Synth. Met.*, **73,** 1 (1995).
26. H. Fujimoto, K. Tokumitsu, A. Mabuchi, T. Kasuh, and M. Shiraishi, *Carbon,* **32,** 1249 (1994).
27. R. Yazami and M. Deschamps, *J. Power Sources,* **54,** 411 (1995).
28. K. Tatsumi, N. Iwashita, H. Sakaebe, H. Shioyama, S. Higuchi, A. Mabuchi, and H. Fujimoto, *This Journal,* **142,** 716 (1995).
29. N. Sonobe, N. Ishikawa, and T. Iwasaki, pp. 47-48, in Extended Abstracts of 35th Battery Symposium in Japan, Nagoya, Japan (1994).
30. F. Tuinstra and J. L. Koenig, *J. Chem. Phys.*, **53,** 1126 (1970).
31. M. Nakamizo, *Tanso,* **90,** 105 (1977).
32. Z. X. Shu, R. S. McMillan, and J. J. Murray, *This Journal,* **140,** 922 (1993).
33. S. A. Solin, *Physica,* **B99,** 443 (1980).
34. J. R. Dahn, A. K. Aleigh, H. Shi, B. M. Way, W. J. Weydanz, J. N. Reimers, Q. Zhong, and U. von Sacken, in *Lithium Batteries,* G. Pistoia, Editor, Chap. 1, Elsevier, Amsterdam (1994).
35. J. Conard and H. Estrade, *Mater. Sci. Eng.*, **31,** 173 (1977).
36. S. A. Solin, in *Graphite Intercalation Compounds I,* H. Zabel and S. A. Solin, Editors, Chap. 5, Springer-Verlag, Berlin (1990).
36. K. Tatsumi, T. Akai, T. Imamura, K. Zaghib, N. Iwashita, S.-I. Higuch, and Y. Sawada, pp. 97-98, in Extended Abstracts for the 36th Battery Symposium in Japan, Kyoto, Japan (1995).

# Electrochemical Studies on $LaNi_{5-x}Sn_x$ Metal Hydride Alloys

**B. V. Ratnakumar***

*Jet Propulsion Laboratory, Electrochemical Technologies Group, Pasadena, California 91109, USA*

**C. Witham,** R. C. Bowman, Jr., A. Hightower, and B. Fultz**

*California Institute of Technology, Division of Engineering and Applied Science, Pasadena, California 91125, USA*

ABSTRACT

Electrochemical studies were performed on $LaNi_{5-x}Sn_x$ with $0 \leq x \leq 0.5$. We measured the effect of the Sn substituent on the kinetics of charge-transfer and diffusion during hydrogen absorption and desorption, and the cyclic lifetimes of $LaNi_{5-x}Sn_x$ electrodes in 250 mAh laboratory test cells. We report beneficial effects of making small substitutions of Sn for Ni in $LaNi_5$ on the performance of the metal hydride alloy anode in terms of cyclic lifetime, capacity, and kinetics. The optimal concentration of Sn in $LaNi_{5-x}Sn_x$ alloys for negative electrodes in alkaline rechargeable secondary cells was found to lie in the range $0.25 \leq x \leq 0.3$.

## Introduction

The use of metal hydrides (MH) as negative electrodes in alkaline rechargeable cells is becoming increasingly popular, owing to advantages of the metal hydrides over conventional anode materials (such as Zn, Cd) in specific energy, cyclic lifetime, and environmental compatibility. The similarities in the cell voltage, pressure characteristics, and charge control methods of the Ni-MH cells to the commonly used Ni-Cd cell suggest that Ni-MH cells may take over a good fraction of the rechargeable battery market for consumer electronics in the next few years.

Two classes of metal hydride alloys currently being developed are those based on rare earth metals ($AB_5$, where A represents a rare earth or early transition metal and B may include any of the late transition or p-shell metals)[1,2] and on early transition metals ($AB_2$)[3]. Although $AB_2$ alloys are reported to exhibit higher specific energy than the $AB_5$ alloys, state-of-the-art commercial Ni-MH cells predominantly use $AB_5$ alloys. The $AB_5$ alloys are based on $LaNi_5$ with various substituents for La and Ni. The systematic effects of these alloy modifications, and the reasons for these effects, are active topics of research. An important goal of an alloy modification is to increase the lifetime of the MH electrode under charge-discharge cycling. It has been found that cyclic lifetime is affected by the alloy modifications, but it is not clear why. Improved cyclic lifetimes with Co substitutions have been attributed to a reduced volume change upon hydrogen absorption and desorption.[1] Sakai *et al.*[4] studied various ternary substitutions for Ni in $LaNi_5$ and reported that cyclic lifetime improves with the ternary substituents studied in the order Mn < Ni < Cu < Cr < Al < Co. It has also been suggested that substitution of the rare earth metal with Ti[5], Zr[6], or other lanthanides such as Nd[1] and Ce[7] may promote the formation of a protective surface film and enhance cyclic lifetime. This is auspicious for the use of relatively inexpensive misch metal, Mm (a naturally occurring mixture of rare earth metals La, Ce, Pr, and Nd), for La in alloy formulations such as $(Mm)(Ni\text{-}Co\text{-}Mn\text{-}Al)_5$.[8,9]

The beneficial effect of the substituents for either La or Ni is often accompanied by an undesirable decrease in hydrogen absorption capacity, long activation, and slow kinetics of hydrogen absorption and desorption. In our recent communications,[10,11] we described the advantages associated with using Sn as a ternary substituent. The addition of small amounts [3.3 atom percent (a/o)] of Sn improves cycle life and the kinetics of absorption and desorption with a marginal reduction in specific capacity. The specific capacity of $LaNi_{4.8}Sn_{0.2}$ is about 300 mAh/g and is retained well during charge-discharge cycling. The benefits of alloying with Sn have also been realized in multicomponent alloys.[12] In this paper, we present results from further studies on the Sn-modified $LaNi_5$ alloys of differing Sn concentrations. These studies were aimed at identifying the effect of the Sn additive on electrochemical characteristics of the metal hydride alloys, including the kinetics of charge-transfer and diffusion during the hydriding process, and cyclic lifetimes in 250 mAh laboratory test cells.

## Experimental

The $LaNi_{5-x}Sn_x$ alloys were prepared by either arc-melting or induction-melting stoichiometric amounts of each metal. Nickel (99.9%) and tin (99.999%) were obtained from Johnson-Matthey, Ward Hill, MA, USA, and lan-

* Electrochemical Society Active Member.
** Electrochemical Society Student Member.

thanum (99.99%) was obtained from Johnson-Matthey, UK. The samples with $x = 0.4$ and 0.5 originally produced by Hydrogen Consultants, Inc., Littleton, CO, were treated in the same manner as all other alloys, which were produced at Caltech. To insure homogeneous distribution of Sn in the alloys, the ingots were subsequently annealed in vacuum at 950°C for 72 h. The annealed ingots were then crushed to 10 mesh in an argon glove box followed by a single hydrogen absorption/desorption cycle to activate the alloys and to obtain alloy powders of optimized surface area. The chemical composition and homogeneity of the alloys were characterized by x-ray diffractometry. X-ray data were obtained with an INEL CPS-120 powder diffractometer using Co $K_\alpha$ radiation ($\lambda = 1.7902$ Å).

Pressure-composition isotherms were obtained for $LaNi_{5-x}Sn_x$ alloys by using a modified gas-manifold Sievert's apparatus described previously.[13] The electrode powder mixture contained 76% MH alloy powder (< 75 μm), 19% INCO nickel powder (1 μm) as a conductive diluent, and 5% Teflon binder. The electrodes for the cyclic lifetime studies (area: 2.54 × 2.54 cm) were fabricated by hot-pressing at 300°C and $6.9 \times 10^7$ Pa approximately 1.3 g of the mixture (~1 g MH powder) onto an expanded Ni screen. For the basic electrochemical studies, recessed cylindrical cavity BAS (Bio-Analytical Systems) disk electrodes were hand-packed with approximately 110 mg of the electrode powder mixture (as in a paste electrode) to ensure consistent values for the electrode area (0.09 $cm^2$) and porosity. NiOOH electrodes from an aerospace Ni-Cd cell, supplied by Eagle-Picher, formed the counterelectrode in each type of cell. A three-electrode flooded open cell with a Luggin capillary for the Hg/HgO reference electrode[14] was adopted for the basic electrochemical studies (basic cell). For the cyclic lifetime studies, the same components were assembled in a prismatic glass cell with a nylon (Pellon 2516) separator. Teflon shims were used to provide adequate compaction to the electrodes. The electrolyte was 31 weight percent (w/o) KOH (5.5 *M*) solution prepared with twice-distilled, low-conductivity water. Although these were not sealed cells, a Viton O-ring seal did enable the cells to reach pressures slightly above atmospheric conditions. Electrochemical measurements (dc) were performed with an EG&G Princeton Applied Research (PAR) 273 potentiostat/galvanostat interfaced to an IBM-PC, using EG&G corrosion software 252. AC impedance measurements were carried out with the EG&G PAR 273 potentiostat and Solartron 1255 frequency-response analyzer, using EG&G impedance Software 388. Cycling of the prismatic cells was carried out with an automatic battery cycler made by Arbin Corp., College Station, TX. The cycling conditions included a discharging step at a constant current of 12.5 mA/$cm^2$ (150 mA/g, C/2 rate, *i.e.*, 2 h discharge) to −0.5 V *vs.* Hg/HgO. Charging at a constant current of 5 mA/$cm^2$ (60mA/g, C/5 rate) was performed to a charge return of 115% to ensure complete charging of the metal hydride electrode.

## Results and Discussion

*X-ray diffractometry.*—X-ray diffractometry was used to characterize the microstructure, measure the lattice parameters, and verify the phase composition of the MH alloy. Figure 1 shows the diffraction patterns of $LaNi_{5-x}Sn_x$ alloys with different Sn compositions, $x$. The x-ray diffraction patterns confirmed that alloys with Sn compositions up to $x = 0.5$ were entirely the $CaCu_5$-type Haucke phase. With increasing Sn concentration, the diffraction peaks shift to smaller angles (as illustrated in the insert), implying an increase in the lattice parameters.

*Isotherms.*—To understand the hydrogen absorption and desorption characteristics of the alloys, pressure-composition isotherms were measured. Such isotherms were obtained both in the gas phase and in the electrochemical environment. In addition, independent measurement of the gas-phase isotherms for several of these same alloys were made by Luo and co-workers.[15,16] Good agreement in the isotherms was found in all cases.

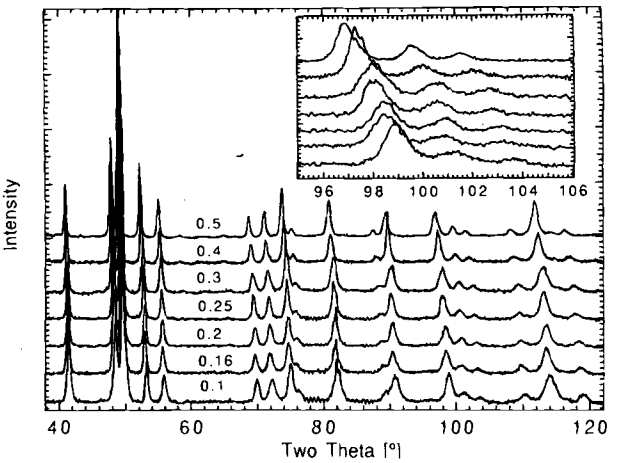


**Fig. 1. X-ray diffraction patterns of $LaNi_{5-x}Sn_x$ alloys. The insert shows the diffraction peaks shifting to smaller angles with increasing Sn composition.**

Electrochemical (EC) isotherms were constructed from the equilibrium electrode potentials at different stages of hydrogen absorption or desorption. These are similar to coulometric titrations carried out on the battery electrode materials.[17] The equilibrium electrode potentials are related to the equilibrium hydrogen pressure,[18] $P_{H_2}$, by the Nernst equation

$$E_o \text{ (vs. HgO/Hg)} = -0.9324 - 0.0291 \log (P_{H_2}) \quad [1]$$

The EC isotherms differ slightly from the gas-phase isotherms during absorption in that the inflection in the pressure at the end of absorption is absent, possibly because internal pressures are limited to 1 atm in the basic cell. The discharge isotherms, on the other hand, bear a greater resemblance to the gas-phase isotherms. The plateau pressures calculated from EC isotherms during charge and discharge are generally comparable to those measured by gas-phase isotherms. Figure 2 shows the EC isotherms during hydrogen absorption (charge) and desorption (discharge) of $LaNi_{5-x}Sn_x$ alloys with $0.1 \leq x \leq 0.3$, along with a representative gas-phase isotherm of $LaNi_5$. The changes in the plateau pressures during absorption and desorption with a change in Sn concentration are shown in Fig. 3.[19] It has been noted that increasing amounts of Sn induce a lattice expansion that is linear

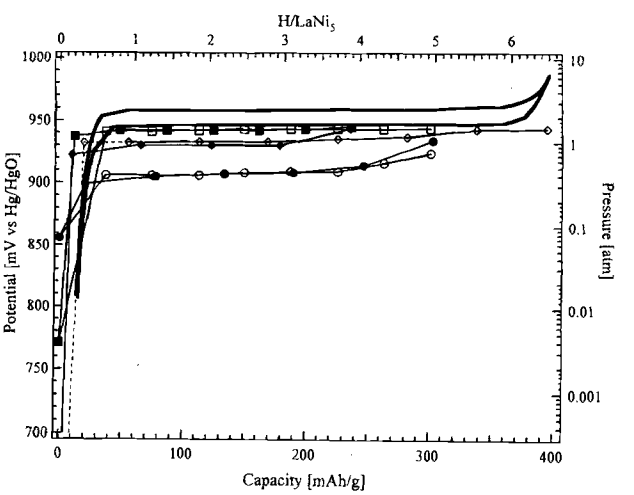


**Fig. 2. Pressure-composition-temperature isotherms of $LaNi_{5-x}Sn_x$ alloys: (—)gas-phase ($-x = 0.0$); and electrochemical: (○, ●) $x = 0.3$; (◇, ◆) $x = 0.2$; (□, ■) $x = 0.1$; open is charge and closed is discharge.**

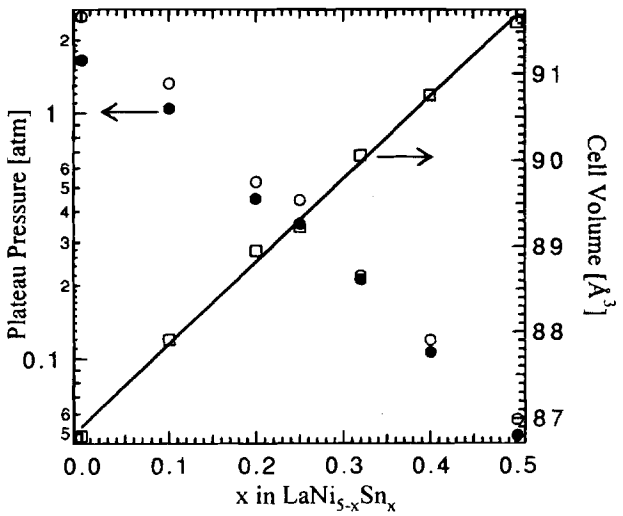


**Fig. 3. Variation with Sn composition, $x$, in $LaNi_{5-x}Sn_x$ alloys of unit cell volume (□) and plateau pressure for 300 K absorption (○) and desorption (●).**

with Sn composition.[20-22] The logarithmic decrease in plateau pressure with increasing unit cell volume seen here is consistent with the observations of Gruen *et al.*[23] As also shown in Fig. 3, the hysteresis between the absorption and desorption isotherms of $LaNi_5$ is reduced in the Sn-substituted alloys.

*Hydrogen absorption capacity.*—The hydrogen absorption capacities of the $LaNi_{5-x}Sn_x$ alloys were measured both in the gas phase and electrochemical environments, as summarized in Fig. 4. Upon Sn substitution, the specific hydrogen absorption capacity calculated for $LaNi_{5-x}Sn_xH_6$ decreases marginally owing to the mass of Sn atoms. As the Sn composition increases, the intrinsic capacity, as measured in the gas phase[15,16,22] is increasingly smaller than these formula values. To determine the discharge capacity, all the electrodes were charged initially at 22 and 5 mA/cm² (22.8 and 60 mA/g) in the disk and prismatic electrodes, respectively, to about 400 mAh/g. This overcharge of about 20 to 40% was used to ensure a complete hydriding of the electrodes. There is no inflection in the charge potentials at the end of charge owing to the hydrogen evolution reaction occurring at the same potentials.

After charging, the disk and prismatic electrodes were discharged at 44.4 and 12.5 mA/cm² (36.4 and 150 mA/g), respectively, to −0.5 V *vs.* Hg/HgO. Discharge capacity improves significantly with the initial increase in Sn composition (Fig. 4). The disparity in measured capacities between basic and prismatic cells could result from a number of factors. The basic cell was limited to atmospheric pressure, while the prismatic cells were able to contain pressures slightly above atmospheric. The capacity for the basic cell is taken from the first cycle, while the prismatic value is taken at the maximum of the cyclic lifetime curve, implying incomplete MH powder activation in the disk electrodes. The disk electrodes were also thicker than those in the prismatic cells (3.175 mm *vs.* ~1 mm) and experienced a larger current density per unit area. The electrochemical capacity of the binary alloy is particularly low. During its charging, significant hydrogen evolution is observed to occur on its surface, which seems to be favored over hydrogen absorption. A similar difficulty in the charging of the binary alloy has been recently reported by Wasz *et al.*, which they overcame by operating their cells at lower temperatures.[22] The maximum discharge capacity measured in prismatic cells was slightly over 300 mAh/g at a discharge rate of C/2, which is an impressive value for an $AB_5$ alloy. For example, some of the state-of-the-art, misch-metal-based, $AB_5$ MH alloys evaluated at Jet Propulsion Laboratory (JPL) showed a maximum capacity of 250 to 275 mAh/g.[24] Apart from ease in chargeability, the low plateau pressures induced by the Sn substitution result in Ni-MH cells of low operating pressures and low self-discharge.

The discharge potentials decrease with an increase in Sn concentration. This is expected from the reduced plateau pressure with increasing Sn concentration in the alloy. The discharge potentials were lower than the equilibrium potentials calculated with Eq. 1. However, the decrease in the electrochemical capacity of alloys with high Sn concentrations is significant compared to the decrease in the calculated capacity or the hydrogen absorption capacities measured with gas-phase isotherms. From an examination of the observed midpoint potentials taken from the dynamic discharge curves in the basic cell and the corresponding equilibrium potentials calculated from the desorption plateau pressures (Fig. 5), it is clear that the discharge overpotentials tend to increase at high Sn compositions, especially for $x > 0.3$. This behavior prompted us to carry out measurements on the kinetics of electrochemical hydriding of $LaNi_{5-x}Sn_x$ alloys.

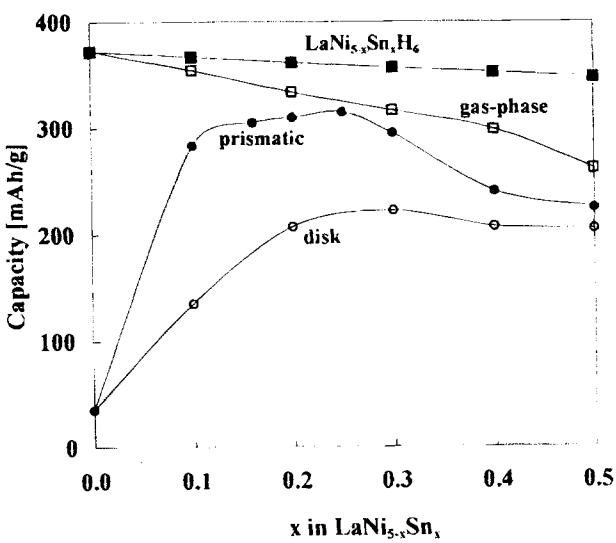


**Fig. 4. Hydrogen absorption capacity of $LaNi_{5-x}Sn_x$ alloys measured with Sieverts' apparatus, prismatic cell electrode, disk electrode, and formula capacity for H/M ratio of 1:1.**

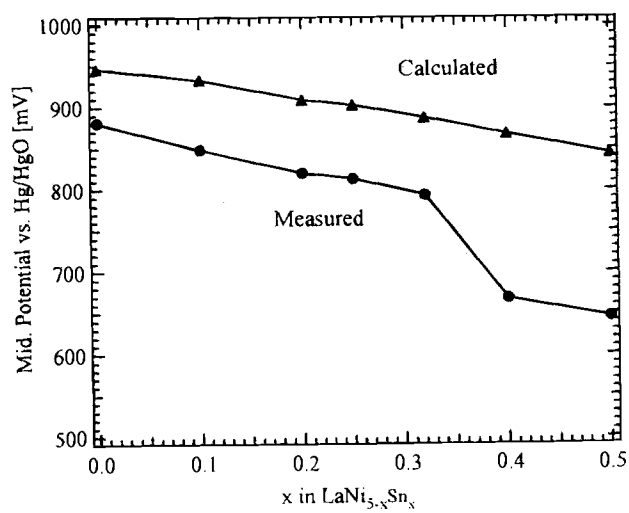


**Fig. 5. Variation of midpoint discharge potentials of disk electrodes and the corresponding equilibrium potentials calculated from the desorption plateau pressures.**

*Kinetics of hydriding.—DC polarization.*—The kinetics of hydrogen absorption/desorption may be slowed by the alloy substituents. For example, elements forming surface films may alter the kinetics of charge-transfer at, or transport of hydrogen through, the surface regions. To determine the effects of the partial substitution of Ni with Sn on the charge and discharge kinetics, dc polarization and ac impedance experiments were performed on disk electrodes made with the MH alloys. Micropolarization and Tafel measurements were performed on the alloys under potentiodynamic conditions at scan rates of 0.02 and 0.5 mV/s, respectively. The scan rates were so chosen to provide near-steady-state conditions with minimal changes in the state of charge of the electrode or its surface conditions. Although these tests were done in open cells, the results should be valid for sealed cells as well, because additional experiments on the $x = 0.2$ alloy have demonstrated that the kinetics as measured by micro- and Tafel polarization are fairly independent of the state of charge of the material.

Figure 6 shows the micropolarization curves of the $LaNi_{5-x}Sn_x$ alloys. These curves are reasonably linear and spread out, owing to the difference in their equilibrium potentials. The potential of the binary alloy is less anodic (negative) than expected from the calculated equilibrium potentials. This may be caused by its lower state of charge in the unsealed cell configuration. The values of the exchange currents estimated from the slopes of micropolarization curves of different MH alloys show an interesting trend (Fig. 7 and Table I). The exchange current ($i_0$) increases initially upon Sn substitution from 0.77 mA for the binary alloy to 1.35 mA for the alloy with $x = 0.1$. Further addition of Sn decreases the exchange current. Nevertheless, the kinetics of Sn-substituted alloys are superior to those of the binary alloy for Sn compositions of $x \leq 0.3$ in unsealed cells. With Sn compositions of $x \geq 0.4$, the kinetics of hydrogen absorption and desorption are slowed considerably and are even slower than in the binary alloy. The increases in the polarization resistance at higher Sn concentrations may be caused by an incomplete activation of the MH alloy, as discussed in the section on cyclic lifetimes.

To determine the kinetics of absorption and desorption, Tafel polarization measurements were made on the $LaNi_{5-x}Sn_x$ alloys. Figure 8 illustrates the Tafel behavior, corrected for mass transfer, of various alloys during charge and discharge. The overpotentials at any current density can be seen to decrease upon the initial substitution of Sn but increase at the highest Sn concentration. The cathodic Tafel plot of the binary alloy is complicated by the hydrogen evolution reaction, which occurs at the same potentials as the hydriding reaction, resulting in two distinct slopes. The simultaneous occurrence of hydrogen evolution may result in fluctuations in the electrode potentials from the continual forming and bursting of hydrogen gas bubbles on the electrode surface. Such problems are fortunately absent with Sn-substituted alloys, and the Tafel curves are more reproducible. In any case, for the Tafel polarization experiments, the potential was scanned from extreme anodic (positive) values to the cathodic (negative) values to avoid the uncertainties arising from hydrogen bubbles adhering to the surface of the MH electrode.

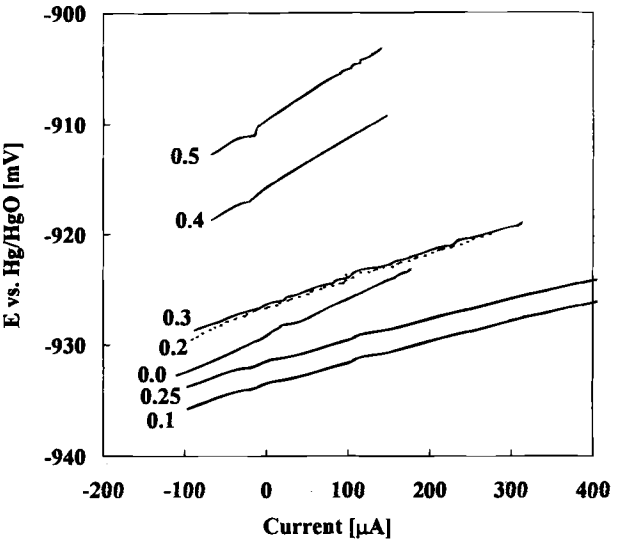


**Fig. 6. Linear polarization curves of $LaNi_{5-x}Sn_x$ alloys.**

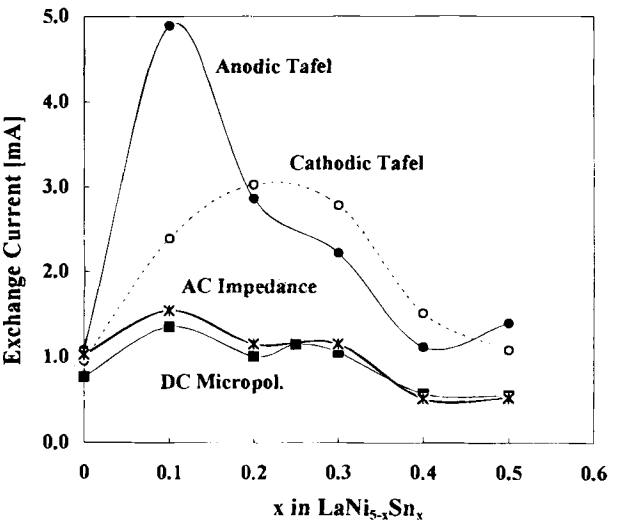


**Fig. 7. Variation of the exchange current density from measurements by dc micropolarization (■), ac impedance (x), anodic Tafel polarization (●), and cathodic Tafel polarization (○).**

The Tafel polarization curves indicate strong mass-transfer effects at high currents. The limiting currents may be related to the slow solid-state diffusion of hydrogen in the MH electrode. The limiting currents are measured in a separate potentiodynamic experiment at a potential 400 mV more positive than the equilibrium potential and are listed in Table I. The diffusion-limiting current on discharge is highest for a Sn composition of $0.1 \leq x \leq 0.2$ (in the range of 500 mA/g) and is reduced at high Sn compositions. Using the measured limiting current, the Tafel plots can be corrected for the mass-transfer effects by

**Table I. Exchange current densities of $LaNi_{5-x}Sn_x$ alloys determined by electrochemical methods.**

| $x$ in $LaNi_{5-x}Sn_x$ | Micropolarization $i_0$ (mA) | Tafel polarization $i_0$ (mA) | | Tafel polarization Slope (mV/dec) | | Discharge limiting current (mA) | AC impedance $i_0$ (mA) |
|---|---|---|---|---|---|---|---|
| | | Abs. | Des. | Abs. | Des. | | |
| 0 | 0.77 | 0.96 | 1.51 | 242 | 108 | 14 | 1.02 |
| 0.1 | 1.35 | 2.39 | 4.89 | 233 | 183 | 480.5 | 1.54 |
| 0.2 | 1.02 | 3.03 | 2.86 | 185 | 220 | 501.7 | 1.15 |
| 0.3 | 1.05 | 2.79 | 2.22 | 173 | 210 | 354.7 | 1.15 |
| 0.4 | 0.57 | 1.51 | 1.12 | 167 | 224 | 251.8 | 0.51 |
| 0.5 | 0.54 | 1.09 | 1.4 | 147 | 229 | 265.6 | 0.52 |

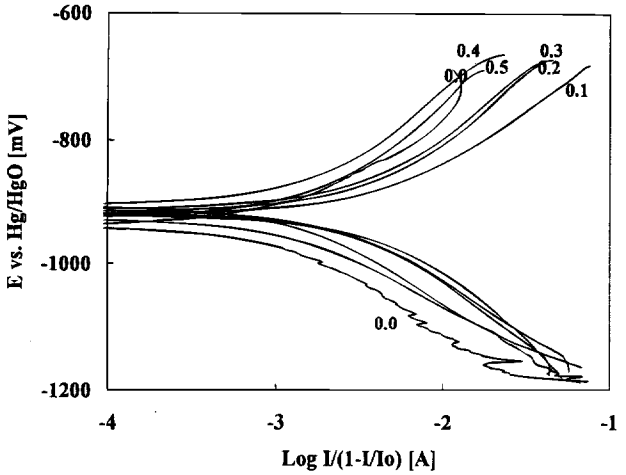


**Fig. 8. Tafel polarization curves with mass-transfer corrections of $LaNi_{5-x}Sn_x$ alloys.**

plotting the logarithm of $I/(1\text{-}I/I_{lim})$ against the electrode potential. The corrected Tafel plots are more linear (Fig. 8). The exchange current density and transfer coefficients for hydrogen absorption were calculated from the intercept and inverse slope of the corrected cathodic Tafel plots, respectively. The corresponding coefficients for hydrogen desorption were calculated from the corrected anodic Tafel plots. The absorption exchange current increases upon Sn substitution and shows a maximum at a Sn composition of $x = 0.2$ (Fig. 7, Table I). The desorption exchange current improves more significantly upon Sn substitution but has a maximum near $x = 0.1$. Nevertheless, the kinetics of desorption continue to be better than the binary alloy for $x < 0.4$. The Tafel slopes show an interesting trend: the slope for the absorption process decreases with increasing Sn concentration, whereas the slope for the desorption process increases (Table I). The change in both the parameters is less marked for $x > 0.2$. It is interesting to note that the equilibrium potentials (calculated from the logarithm of the plateau pressures) also decrease with increasing Sn concentration. It is known[2] that lower plateau pressures facilitate absorption, whereas higher plateau pressures are desirable for desorption. The transfer coefficients during absorption calculated from the Tafel slopes increase with increasing Sn composition from 0.24 for $x = 0$ to 0.25, 0.32, 0.34, 0.35, and 0.4 for $x$ values of 0.1, 0.2, 0.3, 0.4, and 0.5, respectively. The corresponding transfer coefficients during desorption, however, decrease with increasing Sn composition, from 0.55 for $x = 0$ to 0.32, 0.27, 0.28, 0.26, and 0.26.

*AC impedance.*—Electrochemical impedance spectroscopy measurements were made on electrodes in the charged state. The powders were activated by gas-phase absorption but were not electrochemically cycled. The ac impedance data were obtained in the frequency range of 100 kHz to 5 mHz at a low ac amplitude of 2 mV. The impedance plots of $LaNi_{5-x}Sn_x$ alloy electrodes are shown in the Nyquist or Cole-Cole form in Fig. 9. As may be seen in this figure, the impedance decreases noticeably upon initial substitution of Sn but increases for $x \geq 0.4$. The impedance data were analyzed using a generalized equivalent circuit adopted for the MH electrode,[25] shown in the insert. The capacitive components labeled by Q are modeled as constant-phase elements (CPE) to describe the depressed nature of the semicircles.[26] $R_1$ is ascribed to the electrolyte resistance between the MH electrode and the reference electrode. The semicircle in the high-frequency region, represented by $R_2$ and $Q_2$, results from the contact resistance between the current collector and the Teflon-bonded electrode. The contact resistance and capacitance between the particles of the plastic-bonded metal hydride powder generate parameters $R_3$ and $C_3$. The semicircle in the low-frequency region, modeled by $R_4$ and $Q_4$, is attributed to the reaction (charge-transfer) resistance and the double-layer capacitance, respectively. The diffusional impedance, $W_4$, is the Warburg impedance, which is a parallel and/or series combination of diffusional resistance and pseudocapacitance. The observed impedance patterns of the MH electrodes (Fig. 9) are simplified by the absence of a diffusional component. The parameters in the equivalent circuit were calculated by a nonlinear least squares fit using the Boukamp method.[27]

The exchange current calculated from the charge-transfer resistance decreases initially upon substitution of Sn but increases for Sn compositions $x \geq 0.4$ (Table I). The trend is similar to that observed in the dc polarization experiments. It is thus clear that the kinetics of hydriding improve markedly upon Sn substitution in $LaNi_{5-x}Sn_x$, at least for $x \leq 0.3$. Higher amounts of Sn seem to cause sluggish kinetics for hydrogen absorption and desorption. This behavior is currently being studied in more detail.

*Cyclic lifetime.*—Finally, the performance of the MH alloys during charge-discharge cycling was evaluated in 250 mAh, negative-limited, prismatic laboratory test cells. Although sealed cells are typically positive-limited in order to utilize an overcharge mechanism, the present partially sealed cells were designed in the negative-limited configuration (with a deficit of MH) to investigate the life-limiting mechanisms of the MH electrode. The cyclic lifetimes under these accelerated test conditions are expected to be shorter than in sealed commercial cells, but these tests should be appropriate for comparative evaluation of cyclic lifetimes of different metal hydride electrode materials with plateau pressures slightly greater than atmospheric, or less.

The cyclic lifetime of cells containing $LaNi_{5-x}Sn_x$ metal hydride alloys are presented in Fig. 10. This figure shows that the initial capacity increases with an increase in Sn composition. We attribute the lower capacities of the Sn-poor alloys to their high plateau pressures, which were around 1 atm. Since our cells operated only slightly above 1 atm, incomplete charging is expected for the alloys with $x < 0.2$. However, the initial capacity declines again for Sn concentrations higher than 6.7 a/o, or $x \geq 0.4$. While suppressed hydrogen absorption/desorption kinetics could also be responsible for this trend at high Sn concentrations, we attribute this effect to the loss of the intrinsic capacity of the alloy, incomplete activation, and the low desorption pressures of the alloys. As evident in Fig. 4, Sn

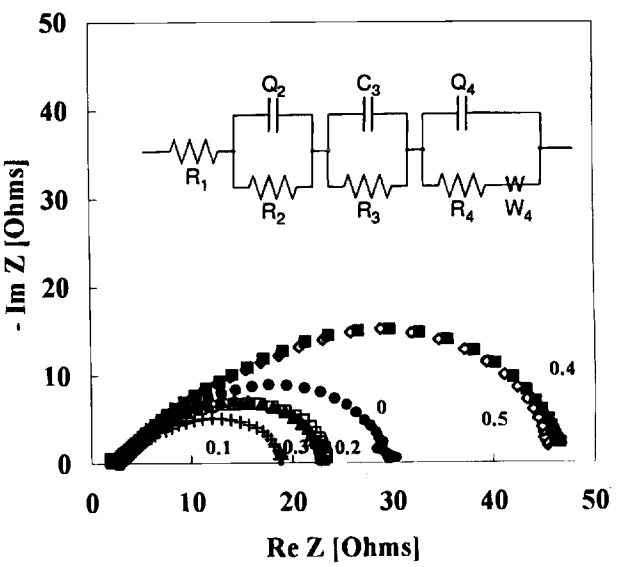


**Fig. 9. Electrochemical impedance spectroscopy (EIS) curves of $LaNi_{5-x}Sn_x$. Insert shows equivalent circuit.**

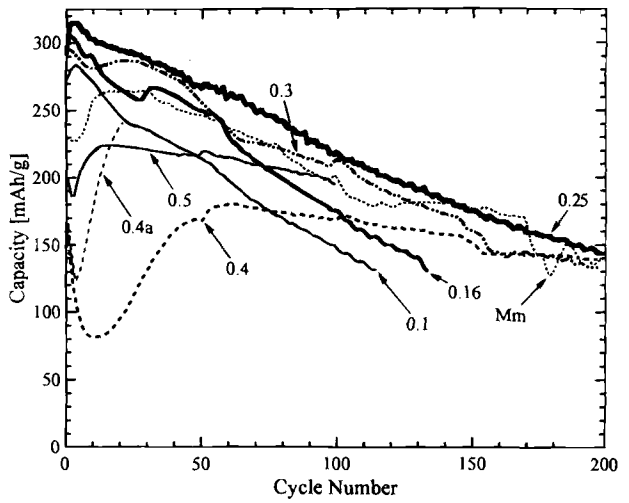


**Fig. 10. Cyclic lifetime behavior of $LaNi_{5-x}Sn_x$ alloys with comparison to the best misch-metal-based, multicomponent alloy evaluated at JPL (Ref. 24).**

compositions of $0.2 \leq x \leq 0.3$ provide the highest initial capacities of approximately 300 mAh/g.

It may be noted that our alloys all experience a shorter cyclic lifetime than those achieved by other experimenters,[12,22] and this can be attributed to the strenuous cycling conditions used to test our cells. The deep discharge to −0.5 V *vs.* Hg/HgO accelerates the loss in capacity,[4] compared to the −0.7 V often used.[12,22] The high applied current density, normalized by area, and the large proportion of active material used in the electrode powder mixture contribute to the effective current density experienced by the MH powders being very large. However, we believe that these factors represent more accurately the lifetime the MH alloys will obtain in cells manufactured for consumer use.

Each cell was subjected to 200 charge-discharge cycles. The retention of capacity was found to improve with increasing Sn composition. After 100 charge-discharge cycles, alloys with $x = 0.25$ or 0.3 exhibit capacities in excess of 200 mAh/g, an impressive number when compared to the state-of-the-art $MmNi_{3.5}Co_{0.8}Mn_{0.4}Al_{0.3}$ MH alloys evaluated at JPL[24] (Mm in Fig. 10). It is interesting to note that alloys with high Sn compositions ($x \geq 0.4$) show long activation cycles; taking longer to achieve maximum capacity than alloys with $x \leq 0.3$. This was confirmed by activating a sample with $x = 0.4$ by thermally cycling it with hydrogen five times before electrochemical cycling. Data from this sample are labeled as 0.4a in Fig. 10. This sample was used for the capacity measurement shown in Fig. 4, but the curve in Fig. 10 labeled 0.4 should be used to study capacity degradation. We are currently studying in more detail how incomplete activation affects the alloys' charge/discharge kinetics, but the present results should be valid for powders with a single gas-phase activation cycle. The lifetime capacity in cells with $x \geq 0.4$ exceeds that of cells with $0.2 \leq x \leq 0.3$, as evidenced by the lifetime curves after 150 cycles.

## Conclusions

The substitution of small amounts of Sn for Ni in $LaNi_5$ improves many characteristics of the metal hydride anode in partially sealed prismatic alkaline rechargeable cells. Specifically, chargeability is improved owing to reduced absorption plateau pressures. The hydrogen absorption capacity of the $LaNi_{5-x}Sn_x$ alloys exceeds 300 mAh/g, an impressive number for an $AB_5$ formulation. The kinetics of hydrogen absorption and desorption are improved markedly compared to the binary alloy, although at high Sn concentrations the improvement is less evident, possibly resulting from incomplete activation. The capacity retention during charge-discharge cycling is significantly enhanced such that the cyclic lifetime of Sn-substituted alloys is comparable to some multicomponent, misch-metal-based alloys. Tin compositions in the range of $0.2 \leq x \leq 0.3$ appear to be optimal for high capacities, long cyclic lifetime, and improved kinetics. We suggest that higher Sn compositions ($0.4 \leq x \leq 0.5$) may be favored for high-temperature applications. The simple alloy chemistry and absence of Co in these alloys gives them an advantage over the $Mm(NiCoMnAl)_5$ alloys now being produced commercially.

## Acknowledgments

This work was carried out at the Jet Propulsion Laboratory under contract with the National Aeronautics and Space Administration (NASA) and at the California Institute of Technology under funding by the Department of Energy (DOE) Grant No. DE-FG03-94ER14493. We thank NASA for providing the facilities for the electrochemical studies and DOE for support for all the authors and the Sievert's apparatus at Caltech. We thank L. A. Wade of JPL for providing samples of several alloys and Professor T. B. Flanagan of the University of Vermont, for supplying detailed results of their isotherm measurements.

Manuscript submitted Oct. 18, 1995; revised manuscript received April 18, 1996.

*California Insitute of Technology assisted in meeting the publication costs of this article.*

REFERENCES

1. J. J. G. Willems, *Philips J. Res.*, **39** (Suppl. 1), 1 (1984); J. J. G. Willems and K. H. J. Buschow, *J. Less-Common Met.*, **129**, 13 (1987).
2. T. Sakai, K. Muta, H. Miyamura, N. Kuriyama, and H. Ishikawa, in *Hydrogen Storage Materials, Batteries, and Electrochemistry*, D. A. Corrigan and S. Srinivasan, Editors, PV 92-5, p. 59, The Electrochemical Society Proceedings Series, Pennington, NJ (1992); T. Sakai, H. Yoshinaga, H. Miyamura, and H. Ishikawa, *J. Alloys Compd.*, **180**, 37 (1992).
3. S. R. Ovshinsky, M. A. Fetcenko, and J. Ross, *Science*, **260**, 176 (1993); M. A. Fetcenko, S. Venkatesan, and S. R. Ovshinsky, in *Hydrogen Storage Materials, Batteries, and Electrochemistry*, D. A. Corrigan and S. Srinivasan, Editors, PV 92-5, p. 141, The Electrochemical Society Proceedings Series, Pennington, NJ (1992); M. A. Fetcenko, S. Venkatesan, K. C. Hong, and B. Reichman, in *Proceedings of the 16th International Power Sources Symposium*, Vol. 12, p. 411, International Power Sources Committee, UK (1988).
4. T. Sakai, K. Oguru, H. Miyamura, N. Kuriyama, A. Kato, and H. Ishikawa, *J. Less-Common Met.*, **161**, 193 (1990).
5. T. Sakai, H. Miyamura, N. Kuriyama, A. Kato, and K. Oguru, *ibid.*, **159**, 127 (1990).
6. T. Sakai, H. Miyamura, N. Kuriyama, A. Kato, K. Oguru, and H. Ishikawa, *This Journal*, **137**, 795 (1990).
7. T. Sakai, T. Hazama, H. Miyamura, N. Kuriyama, A. Kato, and H. Ishikawa, *J. Less-Common Met.*, **172-174**, 1175 (1991).
8. N. Furukawa, *J. Power Sources*, **51(1-2)**, 45 (1994).
9. K. Suzuki, N. Yanagihara, H. Kawano, and A. Ohta, *J. Alloys Compd*, **192**, 173 (1993).
10. B. V. Ratnakumar, G. Halpert, C. Witham, and B. Fultz, *This Journal*, **141**, 189 (1994).
11. B. V. Ratnakumar, S. Surampudi, S. Di Stefano, G. Halpert, C. Witham, A. Hightower, and B. Fultz, in *Hydrogen and Metal Hydride Batteries*, P. D. Bennett and T. Sakai, Editors, PV 94-27, p. 57, The Electrochemical Society Proceedings Series, Pennington, NJ (1994).
12. A. Anani, A. Visintin, K. Petrov, and S. Srinivasan, *J. Power Sources*, **47**, 261 (1994); W. Zhang, M. P. S. Kumar, S. Srinivasan, and H. J. Ploehn, *This Journal*, **142**, 3424 (1994).
13. R. C. Bowman , Jr., C. H. Luo, C. C. Ahn, C. K. Witham, and B. Fultz, *J. Alloys Compd*, **217**, 185 (1995).
14. B. V. Ratnakumar, S. Di Stefano, S. Surampudi, and G. Halpert, *This Journal*, **143**, 803 (1996).

15. S. Luo, W. Luo, J. D. Clewley, T. B. Flanagan, and R. C. Bowman, *J. Alloys Compd*, **231**, 473 (1995).
16. S. Luo, W. Luo, J. D. Clewley, T. B. Flanagan, and L. A. Wade, *ibid.*, **231**, 467 (1995).
17. For example, A. Anani and R. A. Huggins, *J. Power Sources*, **38**, 363 (1992).
18. C. Jordy, A. Percheron-Guegan, J. Bouet, P. Sanchez, C. Chanson, and J. Leonardi, *J. Less-Common Met.*, **172-174**, 1236 (1991).
19. T. B. Flanagan, Personal communication.
20. M. Mendelsohn, D. Gruen, and A. Dwight, *Inorg. Chem.*, **18**, 3343 (1979).
21. J. S. Cantrell, T. A. Beiter, and R. C. Bowman, Jr., *J. Alloys Compd*, **207/208**, 372 (1994).
22. M. Wasz, R. B. Schwarz, S. Srinivasan, and M. P. S. Kumar, in *Materials for Electrochemical Energy Storage and Conversion-Batteries, Capacitors, and Fuel Cells*, Symposium Proceedings of The Materials Research Society, MRS, Pittsburgh, PA (1996).
23. D. N. Gruen, M. H. Mendelsohn, and A. E. Dwight, *J. Less-Common Met.*, **63**, 193 (1979).
24. B. V. Ratnakumar, S. Surampudi, S. Di Stefano, and G. Halpert, in *Proceedings of the 36th Power Sources Conference*, p. 202, Electronic and Power Sources Directorate, U.S. Army Research Laboratory, IEEE, New York (1994).
25. N. Kuriyama, T. Sakai, H. Miyamura, I. Uehara, and H. Ishikawa, *J. Alloys Compd.*, **192**, 161 (1993).
26. J. Ross McRonald, *Impedance Spectroscopy*, John Wiley & Sons, New York (1987).
27. B. A. Boukamp, *Solid State Ionics*, **20**, 31 (1986).

# Electrodeposition of Fe-C Alloys from Baths Containing Dicarboxylic Acids with a Linear Alkyl Chain

**Yutaka Fujiwara,*[a] Tomio Nagayama,[b,e] Akira Nakae,[c] Masanobu Izaki,[a] Hidehiko Enomoto,[a] and Eiko Yamauchi[d]**

[a]*Osaka Municipal Technical Research Institute, 1-6-50 Morinomiya, Joto-ku, Osaka 536, Japan*
[b]*Graduate School, Kansai University, 3-3-5 Yamate-cho, Suita-city, Osaka 564, Japan*
[c]*Fuso Chemical Company, Limited, 2-2-6 Niitaka, Yodogawa-ku, Osaka 532, Japan*
[d]*Department of Materials Science and Engineering, Kansai University, 3-3-5 Yamate-cho, Suita-city, Osaka 564, Japan*

ABSTRACT

Fe-C alloys were electrodeposited at high current efficiencies from $FeSO_4$ solutions containing a dicarboxylic acid with a linear alkyl chain, represented by $COOH \cdot (CH_2)_n \cdot COOH$ ($n$ = 0 to 7). The carbon contents of the deposits ranged from 0.1 to 3.7 weight percent (w/o), depending on the acid added to the bath. The hardness of the deposits sharply increased to a maximum value of HV 850 with increasing carbon content up to 0.6 w/o and progressively decreased at higher carbon contents. The deposits having carbon contents above 0.5 w/o exhibited a black color, because carbon-rich alloys deposited through the black oxide films in a state similar to FeO containing an organic acid or its degradation products. Fe-C alloy deposits had a body-centered tetragonal, martensite-type lattice with interstitial carbon atoms, and the axial ratios increased with increasing carbon content of the deposits. The high hardness of the Fe-C alloy deposits is mainly attributed to the solid solution hardening by interstitial carbon atoms in the martensite-type lattice. The larger grain size and FeO occluded in the bulk of the carbon-rich deposits caused the decrease in hardness with increasing carbon content.

Fe-C alloys containing 0.4 to 1.3 w/o carbon are electrodeposited from $FeSO_4$ solutions with a small amount of citric acid and l-ascorbic acid. This type of bath, first proposed by Izaki *et al.*[1-3] is abbreviated as the C-A bath. Fe-C alloy electrodeposits from the C-A bath show high hardness above HV 800, a smooth surface and a black color, and have a body-centered tetragonal martensite-type lattice.[1,3,4]

Fe electrodeposition has been used for various engineering applications such as glass molds, soldering iron tips, electroforming, and repairing worn parts where wear resistance is required.[5,6] Nevertheless, fairly low hardness of commercially electroplated Fe ranging from HV 150 to 500[5] leads to insufficient wear resistance. Therefore, Fe-C alloy electrodeposits have potential for commercial use as an alternative to the Fe electrodeposits in engineering applications because of their high hardness. Fe-C alloy electrodeposits are also under evaluation as an alternative to thermal surface hardening processes such as carburizing or nitriding because the hardness of the deposits is comparable to these processes.

We[7] have reported previously that Fe-C alloys are also electrodeposited from baths containing a hydroxy-polycarboxylic acid, namely, l-malic acid, l-tartaric acid, or citric acid without the addition of l-ascorbic acid. Fe-C alloy deposits obtained from these baths showed a black color and a tetragonal martensite-type lattice[7] similar to those from the C-A bath.[1,3,4] These results suggest that the hard Fe-C alloys are also electrodeposited from baths containing other organic acids.

The aim of this work is to elucidate the essential bath constituents for the hard Fe-C alloy plating and to obtain fundamental information for further study of carbon codeposition mechanisms. We selected dicarboxylic acids with a linear alkyl chain, represented by $COOH \cdot (CH_2)_n \cdot COOH$ where $n$ = 0 to 7, as the carbon source of the deposits. We have studied the electrodeposition of Fe-C alloys from baths with these acids and discuss the effects of alkyl chain length of the acids on the nature of the deposits with regard to carbon content, oxygen content, hardness, surface morphology, microstructure, and crystal structure. We have also studied the nature of the deposits compared with that from the C-A bath and Fe deposits.

## Experimental

Baths were prepared from reagent-grade chemicals and deionized distilled water and contained 0.14 mol/dm$^3$ $FeSO_4$ and $5.4 \times 10^{-3}$ mol/dm$^3$ of one of the organic acids. These concentrations are the same as those of the C-A bath, although l-ascorbic acid was not added. The dicarboxylic acids, $COOH \cdot (CH_2)_n \cdot COOH$, used in this work were oxalic acid ($n$ = 0), malonic acid ($n$ = 1), succinic acid ($n$ = 2), glutaric acid ($n$ = 3), adipic acid ($n$ = 4), pimelic acid ($n$ = 5), suberic acid ($n$ = 6), and azelaic acid ($n$ = 7).

* Electrochemical Society Active Member.
[e] Present address: Kyoto Municipal Institute of Industrial Research, 17 Chudoji Minami-machi, Shimogyo, Kyoto 600, Japan.